1-D Fast Neutron Source Localization Using Digital Pixelated 3-D Position-Sensitive CdZnTe Detectors

David Goodman, Michael Streicher, Yuefeng Zhu, Steven Brown, and Zhong He, *Senior Member, IEEE*

***Abstract*— Recoil of constituent nuclei from neutron elastic scatter in pixelated, 3-D CdZnTe gamma-ray detectors is detectable given current low energy thresholds. Fast neutrons are attenuated by CdZnTe detectors via outscatter and measured gradients in neutron interaction rates across detector pixels that enables 1-D fast neutron source localization through a maximum likelihood estimator. Experimental results using an MP320 deuterium–deuterium neutron generator with the four detector crystal Orion prototype successfully localize four different source locations across a 1-D field of view to within absolute measurement errors between 2.5° and 14.0°.**

***Index Terms*— 3-D CdZnTe, digital ASIC, fast neutron detection, fast neutron localization.**

I. Introduction

DETECTION of special nuclear material (SNM) is of national security concern. Recently, 3-D pixelated CdZnTe has been used as a high energy resolution, room-temperature operation, fieldable gamma-ray imaging spectrometer capable of detecting and characterizing SNM [1], [2]. The prominent SNM gamma rays are 186 keV from ^{235}U and less than 450 keV from ^{239}Pu, which are easily shielded by high-Z materials, making them challenging to detect. Sensitivity to fast neutrons offers a complementary signal, as fast neutrons can penetrate high-Z materials. Furthermore, attempts to attenuate fast neutrons via moderation will still produce signal in CdZnTe from thermal capture on ^{113}Cd [3], [4]. Recent advancement in the digital readout technology has pushed low energy thresholds below 5 keV allowing for the detection of nuclear recoils from elastic neutron scatter [5]. Using detector attenuation across detector voxels, fast neutron sources can coarsely be localized in 1-D using CdZnTe. With combined fast neutron and gamma-ray localization capabilities, thermal neutron sensitivity, and $<1\%$ gamma-ray energy resolution at room temperature, CdZnTe detectors offer unique detection capabilities for SNM.

Manuscript received February 2, 2017; revised June 23, 2017; accepted July 15, 2017. Date of publication July 20, 2017; date of current version September 14, 2017. This work was supported in part by the National Science Foundation Graduate Research Fellowship under Grant DGE 1256260 and in part by the U.S. Department of Defense, Defense Threat Reduction Agency under Award HDTRA1-12-C-0034. *(Corresponding author: David Goodman.)*

The authors are with the Department of Nuclear Engineering and Radiological Sciences, University of Michigan, Ann Arbor, MI 48109 USA (e-mail: digoodma@umich.edu).

Color versions of one or more of the figures in this paper are available online at http://ieeexplore.ieee.org.

Digital Object Identifier 10.1109/TNS.2017.2729942

Traditionally, fast neutrons are detected using hydrogenous detectors, such as liquid or plastic scintillators, where fast neutrons are distinguished from gamma-rays via pulse shape discrimination (PSD) [6]. Once detected, several fast neutron source localization methods have been developed using a variety of techniques, such as spatial coded aperture, time encoded imaging, neutron scatter kinematics, and detector self-attenuation. In spatial coded aperture systems, a hydrogenous mask is placed between the source and the detector, casting a unique shadow on a position-sensitive detector, where a decoding function can then be used to deconvolve source direction [7]. In time encoded imaging techniques, source counts are temporally modulated by moving a hydrogenous mask, where source positions are similarly decoded with an associated function [8]. Neutron scatter cameras leverage scatter kinematics to electronically collimate valid source directions to the surfaces of rings [9], [10]. Detector self-attenuation has been used to localize sources using an array of position insensitive detectors, where ratios of detector count rates are used to localize sources [11]. Furthermore, detector arrays can be rotated to record count rates as a function varied geometries to enhance localization and mitigate the lack of position sensitivity within detector volumes [12]. Attenuation has been previously used in a single, pixelated HgI_2 detector to localize gamma-ray sources by recording count rate gradients across detector voxels [13]. Although a nontraditional neutron detector, the fine detector position resolution of pixelated CdZnTe allows for the detection of small neutron count rate gradients, which can be similarly used to localize sources. With the addition of multiple of CdZnTe crystals in an array, fast neutron source localization and sensitivity can be enhanced.

II. Fast Neutron Signal

Unlike organic scintillators with PSD, most fast neutron and gamma-ray interactions are not distinguishable on an event-by-event basis in CdZnTe. Therefore, neutron gamma-ray discrimination is done in CdZnTe via energy windowing. Fast neutrons interact with CdZnTe through primarily inelastic and elastic scattering. During inelastic scatter, fast neutrons excite the target nucleus while depositing some kinetic energy. The excited target subsequently deexcites emitting a characteristic gamma-ray. In an elastic scatter, the fast neutron scatters off a target nucleus, depositing kinetic energy as a function of

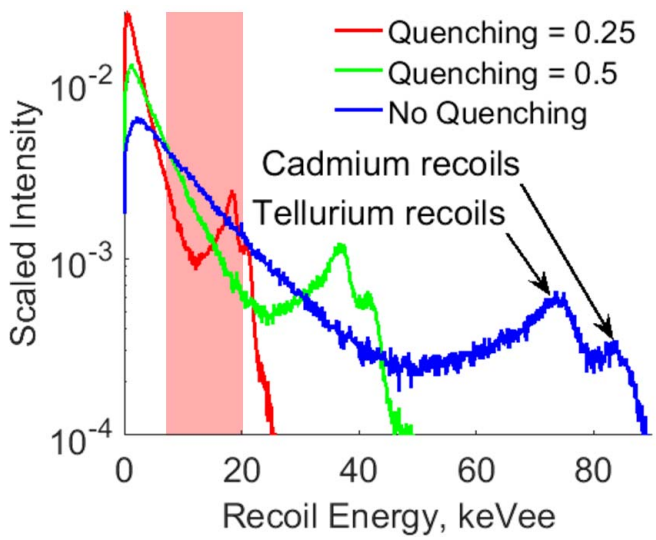

Fig. 1. Simulated relative recoil spectra from a 2.5-MeV neutron source with and without quenching. The energy bin used to tag neutron scatters in CdZnTe is highlighted in red.

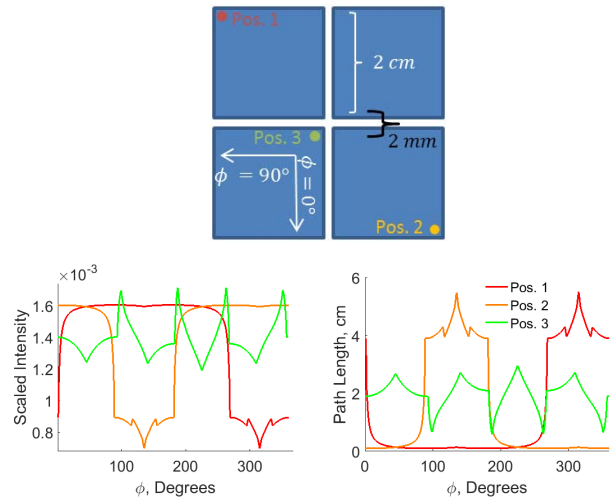

Fig. 2. Top: three hypothetical fast neutron scatters recorded in a four crystal CdZnTe system. Bottom: path lengths x^d (left) and relative incident neutron direction probabilities (right) for each event calculated through the first-order attenuation model. Path length fluctuations in position three are caused by detector gaps.

scatter angle. The recoil spectrum for 2.5-MeV neutrons in CdZnTe is shown in Fig. 1. The recoil energies are further reduced by a quenching factor between 0.25 and 0.5 due to the enhanced recombination of electron–hole pairs from the high charge density produced by high stopping power recoils [5]. This quenching greatly reduces total system sensitivity causing CdZnTe with 5-keVee thresholds, the energy deposition equivalent to a 5-keV electron, to be primarily sensitive to backscatter events. All interactions falling in 5–20-keVee bin are labeled as neutron interactions and used in subsequent angular localization reconstructions. Detector housings block low-energy X-rays causing the primary contamination of this energy bin to be from the small angle scatters of high-energy gamma-rays.

III. Localization Technique

Neutrons with 2.5 MeV interact via inelastic and elastic scattering with CdZnTe crystals. These crystals modulate the incident flux with a macroscopic cross section $\Sigma_T \simeq 0.15\ \text{cm}^{-1}$. Due to the complex nature of neutron scatter kinematics, a first-order model was implemented assuming any interaction removes neutrons from the system, preventing subsequent signals. Notably, this approximation overestimates detector attenuation. Using this model, the probability p, an interaction in detector pixel n at position $\bar{r}_n$, was emitted from the azimuthal direction ϕ as follows:

$$p_n(\phi) = e^{-x(\bar{r}_n,\phi)\Sigma_T} \tag{1}$$

where $x(\bar{r}_n, \phi)$ is the ray traced path length through all CdZnTe from pixel location $\bar{r}_n$ in direction ϕ and Σ_T is the macroscopic cross section for fast neutron interactions in CdZnTe. Sample distributions $p(\phi)$ for three detector pixels in a four crystal array are shown in Fig. 2. Ray traced responses from all detector pixels were then used to predict expected detector pixel counts

$$\boldsymbol{E}[\boldsymbol{g}|\phi_j] = \boldsymbol{\lambda}_j \tag{2}$$

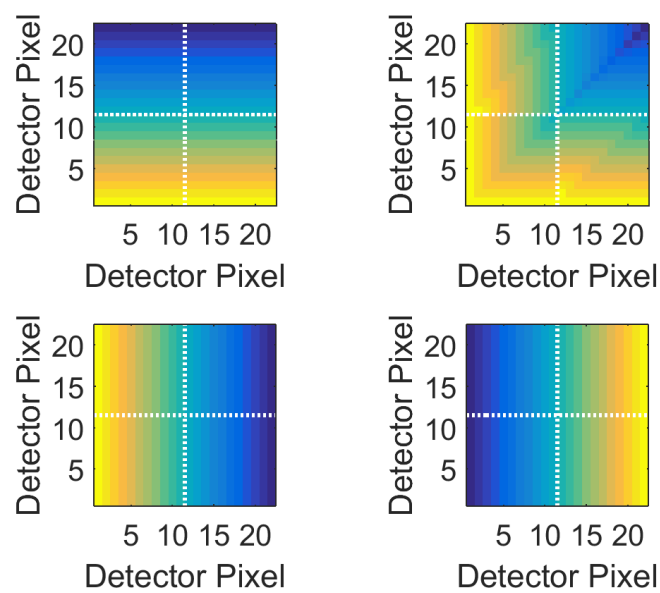

Fig. 3. From top left to bottom right: expected pixel counts $\boldsymbol{\lambda}$ for source directions $\phi = 0°, 45°, 90°, 270°$, given uniform detector sensitivity. Note the clear attenuation of neutron counts across the detector volume. White dashed line: individual detectors, with 11×11 anodes.

for a given source direction ϕ_j. Note that expectation means from all directions are scaled to measure counts. Example expectations are shown in Fig. 3. Model mismatch stemming from the first-order attenuation model was investigated via simulation in GEANT4, as shown in Fig. 4, but chosen as acceptable [14]. These expectations were then sensitivity corrected via a cathode flood, where all detector pixels were evenly illuminated, as shown in Fig. 5. Using these expectations, a maximum likelihood estimator, assuming a single-source direction, was implemented. The likelihood a source in position ϕ_j produced detector pixel counts $\boldsymbol{g}$ given

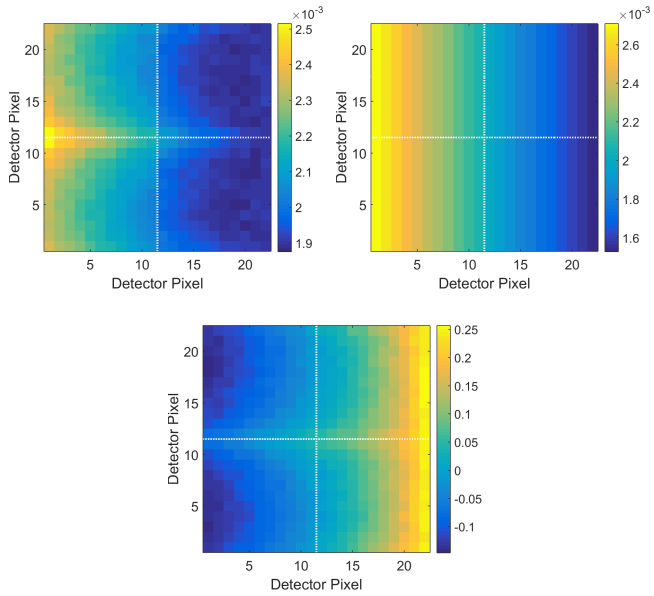

Fig. 4. $\boldsymbol{\lambda}$ for $\phi = 90°$ simulated using GEANT4 (left) and the first-order attenuation model (right) with fractional differences (bottom). Systematic overestimation of attenuation is seen across the detectors yielding a maximum 25% bias.

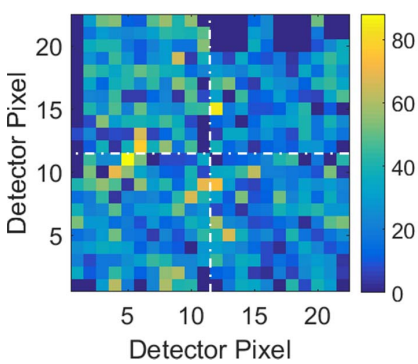

Fig. 5. Pixel sensitivity s_n measured using a cathode illumination where each pixel was exposed to a similar fast neutron fluence. White dashed lines: individual detectors. Pixels with zero counts were disabled due to poor noise performance: individual pixel thresholds can only be slightly changed from a global detector threshold. Note that Poisson uncertainties in pixel sensitivities are large.

expectation $\boldsymbol{\lambda}_j$ is

$$L(\boldsymbol{g}|\boldsymbol{\lambda}_j) = \prod_{n=1}^{N} \frac{\lambda_n^{g_n} e^{-\lambda_n}}{g_n!} \tag{3}$$

where λ_n is the expected number of counts in detector pixel n, g_n is the recorded counts in detector pixel n, and there are N total active detector pixels. For the ease of computation, the natural logarithm was taken for the log-likelihood

$$l(\boldsymbol{g}|\boldsymbol{\lambda}_j) = \sum_{n=1}^{N} g_n \ln(\lambda_n) - \lambda_n \tag{4}$$

where the maximum across J possible, discrete source directions

$$\hat{\phi}_{\text{est}} = \max_{j \in [1,2,\ldots,J]} \{l(\boldsymbol{g}|\boldsymbol{\lambda}_j)\} \tag{5}$$

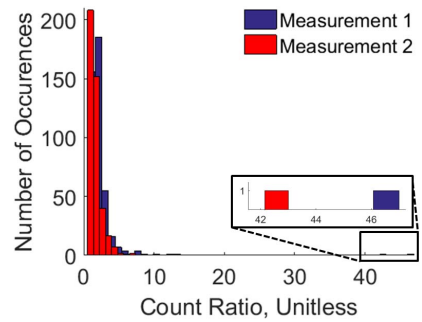

Fig. 6. Sensitivity scaled counts histogrammed for all 484 detector pixels. Clear outliers, boxed in black, with vastly increased sensitivity scaled counts, when compared against other pixels, are seen.

was used as a scalar estimate of the source direction ϕ with the estimator error ϵ_ϕ defined as

$$\epsilon_\phi = |\hat{\phi}_{\text{est}} - \phi_{\text{true}}|. \tag{6}$$

Elastic neutron scatter cross sections increase for fission energies, roughly 1 MeV, and decrease toward 5 MeV. This suggests that count rate gradients used for localization would be enhanced for fission neutrons and degraded for harder sources such as PuBe.

Detector leakage current was found to be slightly time-dependent. This change as a function of time could affect observed pixel trigger rates. Sensitivity scaled pixel counts were histogrammed for localization measurements and outliers were clearly identified as shown in Fig. 6. After identification, the noisy pixel was removed from reconstructions. The pixel with increased noise triggering was shared between measurements and occurred on a detector corner. The hypothesized source of the temporal noise behavior stems from humidity and temperature fluctuations modifying leakage to detector guard rings.

Fast neutron localization using attenuation in current pixelated CdZnTe systems is limited to 1-D due to the lack of depth information for interactions. For gamma-ray interactions, depth is computed using the cathode-to-anode ratio [15]. However, cathode electronic noise degrades depth resolution for small, 5-keVee neutron scatter pulses. This depth uncertainty blurs count rate gradients, making source localization using attenuation along depth difficult.

IV. Detector System

The digital Orion prototype system was used to conduct all measurements [16]. The detector system utilizes four $2 \times 2 \times 1.5$ cm^3 position-sensitive, CdZnTe detectors in a 2×2 array read out by VAD_UMv1.2 digital application-specific integrated circuits (ASICs) [17]. The system is housed in a plastic Pelican case with a Peltier cooler and an aluminum heatsink to remove ASIC heat, as shown in Fig. 7. Detector anodes are pixelated in an 11×11 grid while a planar cathode is used. Lateral interaction location is determined by anode pixels while depth is determined by the cathode-to-anode ratio. Multiple interactions in a single detector or across detectors are recorded in coincidence for a total active volume of 24 cm^3.

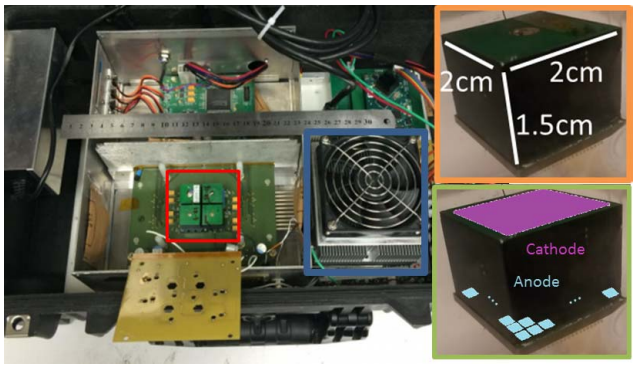

Fig. 7. Four detector digital Orion prototype system housed in a Pelican case with the 2×2 crystal array boxed in red. Inset in orange is a typical $2 \times 2 \times 1.5$ cm^3 CdZnTe crystal. Inset in green is the pixelated anode and planar cathode electrode configuration. The aluminum heat sink for removing ASIC heat is boxed in blue.

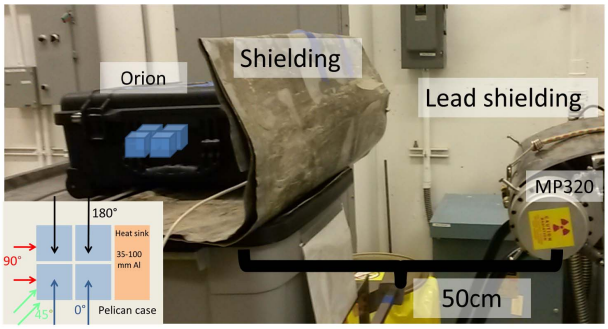

Fig. 8. Relative geometry between the MP320 generator and the Orion prototype with the relative position of crystals shown in blue. Inset: fast neutron irradiation directions of Orion used in subsequent measurements.

Orion energy resolution for ^{137}Cs is roughly ~0.6% FWHM for all events with 300 μm lateral subpixel resolution.

V. Experimental Setup

A Thermo-Fisher MP320 deterium–deuterium (DD) neutron generator was used to illuminate the Orion system with roughly mono-energetic 2.45-MeV neutrons. The DD generator ran at 80 kV with a tube current of 60 μA. Nominal neutron flux was estimated as 10^6n/s into 4π. Significant levels of bremsstrahlung radiation were generated by the movement of deuterium ions and were mitigated by covering the generator with thin layers of lead. Before neutron measurements, a ^{133}Ba source was placed on the generator to confirm that its 80-keV emission was adequately shielded. The generator and the detector system were elevated to reduce the amount of environmental capture gamma-rays and room scattered neutrons. First, a sensitivity measurement was taken by illuminating the cathode side of all crystals uniformly for 45 min. Then, the Orion prototype system was placed 50 cm away from the MP320 target plane with detector sides, not cathodes or anodes, facing toward the generator, as shown in Fig. 8. Each side irradiation was conducted for 45 min with the Orion prototype being rotated laterally between measurements.

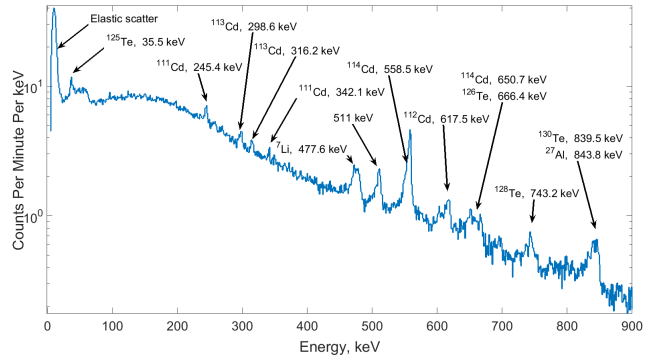

Fig. 9. Background subtracted MP320 spectrum summed across all measurements. Several prominent environmental and detector inelastic and capture gamma-rays are seen.

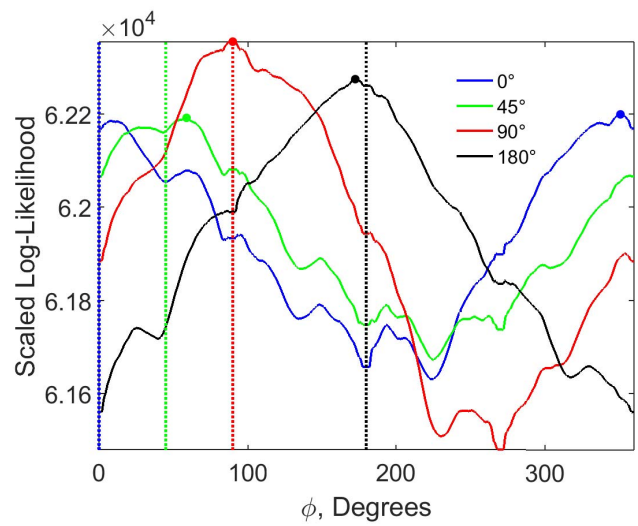

Fig. 10. Log-likelihoods reconstructed using all events in the 5–20-keV window for each illumination angle. Log-likelihoods were scaled to have the same mean for the ease of plotting. Estimated locations are marked with equivalently colored points. Dotted lines: true source locations.

VI. Recorded Energy Spectrum

An overnight background, with no MP320 generator, and spectrum while the generator was running were collected. A background subtracted generator spectrum was then calculated, as shown in Fig. 9. A clear peak in the 5–15-keV region is seen from elastic energy neutron scatters. Notably, this peak is actually a continuous upward trend toward low energy convolved with pixel-to-pixel thresholding effects. Prominent inelastic gamma-ray lines from cadmium and tellurium are seen. Furthermore, the inelastic 558- and 651-keV lines are enhanced from the capture of environmentally thermalized source neutrons on ^{113}Cd.

VII. Source Reconstructions

The log-likelihoods for each illumination angle shown in the inset of Fig. 8 are shown in Fig. 10 over 0.5° bins. An irradiation from 270° was taken but omitted due to the attenuation from the aluminum heatsink. Directional estimates $\hat{\phi}_{\text{est}}$ and associated errors ϵ_ϕ were tabulated in Table I. Discontinuities

TABLE I

TRUE AND ESTIMATED SOURCE LOCATIONS USING A MAXIMUM LIKELIHOOD ESTIMATOR AND FIRST-ORDER ATTENUATION MODEL

ϕ_{true}, °	$\hat{\phi}_{est}$, °	$\lvert\hat{\phi}_{est}-\phi_{true}\rvert$, °
0.0	352.5	7.5
45.0	59.0	14.0
90.0	87.5	2.5
180.0	172.5	7.5

occurring at several angles across reconstructions stem from clusters of pixels disabled due to poor noise performance being excluded from the likelihood. The absolute error of the estimator was between 2.5° and 14.0° even given large uncertainties in pixel sensitivities from Poisson error and use of a naive attenuation model.

VIII. CONCLUSION

Recent improvements in the VAD_UM digital ASIC system for pixelated CdZnTe have decreased low energy thresholds, such that Cd and Te nuclear recoils from fast neutron scatter are detectable. The attenuation of fast neutrons across detectors enables 1-D source localization through a maximum likelihood estimator even with moderate model mismatch from using a naive attenuation model. Differences in pixel-to-pixel detector thresholds require a sensitivity correction, which can be accomplished via a flood irradiation. Due to extreme, low energy thresholds, small, time-dependent shifts in anode noise levels must be monitored occasionally requiring the disabling of previously well behaved pixels. Using measured data from the four crystal Orion prototype system, the direction of a MP320 neutron generator was successfully localized to an absolute error between 2.5° and 14.0° at a distance of 50 cm across a 1-D field of view.

ACKNOWLEDGMENT

The authors would like to thank their current colleagues from the Orion Radiation Measurement Group and past group members whose work they leverage. They would also like to thank Prof. I. Jovanovic for providing MP320 measurement time. Any opinions, findings, and conclusions or recommendations expressed in this material are those of the authors and do not necessarily reflect the views of the Defense Threat Reduction Agency.

REFERENCES

[1] C. G. Wahl *et al.*, "The polaris-H imaging spectrometer," *Nucl. Instrum. Methods Phys. Res. A, Accel. Spectrom. Detect. Assoc. Equip.*, vol. 784, pp. 377–381, Jun. 2015.

[2] M. Streicher, S. Brown, Y. Zhu, D. Goodman, and Z. He, "Special nuclear material characterization using digital 3-D position sensitive CdZnTe detectors and high purity germanium spectrometers," *IEEE Trans. Nucl. Sci.*, vol. 63, no. 5, pp. 2649–2655, Oct. 2016.

[3] D. S. McGregor, J. T. Lindsay, and R. W. Olsen, "Thermal neutron detection with cadmium$_{1-x}$ zinc$_x$ telluride semiconductor detectors," *Nucl. Instrum. Methods Phys. Res. A, Accel. Spectrom. Detect. Assoc. Equip.*, vol. 381, nos. 2–3, pp. 498–501, 1996.

[4] A. Martin-Martin, E. Gallego, R. Barquero, A. Lorente, J. Morcho, and G. Quincoces, "Evaluation of CdZnTe as neutron detector around medical accelerators," *Radiat. Protection Dosimetry*, vol. 133, no. 4, pp. 193–199, 2009.

[5] M. Streicher, D. Goodman, Y. Zhu, S. Brown, S. Kiff, and Z. He, "Fast Neutron Detection using Pixelated CdZnTe Spectrometers," *IEEE Trans. Nucl. Sci.*, vol. 64, no. 7, pp. 1920–1926, Jul. 2017.

[6] F. D. Brooks, "A scintillation counter with neutron and gamma-ray discriminators," *Nucl. Instrum. Methods*, vol. 4, no. 3, pp. 151–163, 1959.

[7] P. A. Hausladen, M. A. Blackston, E. Brubaker, D. L. Chichester, P. Marleau, and R. J. Newby, "Fast-neutron coded-aperture imaging of special nuclear material configurations," in *Proc. 53rd Annu. Meeting Inst. Nucl. Mater. Manage.*, Jul. 2012, pp. 1–10.

[8] P. Marleau *et al.*, "Time encoded fast neutron/gamma imager for large standoff SNM detection," in *Proc. IEEE Nucl. Sci. Symp. Med. Imag. Conf.*, Oct. 2011, pp. 591–595.

[9] A. Poitrasson-Rivière, M. C. Hamel, J. K. Polack, M. Flaska, S. D. Clarke, and S. A. Pozzi, "Dual-particle imaging system based on simultaneous detection of photon and neutron collision events," *Nucl. Instrum. Methods Phys. Res. A, Accel. Spectrom. Detect. Assoc. Equip.*, vol. 760, pp. 40–45, Oct. 2014.

[10] J. E. M. Goldsmith, M. D. Gerling, and J. S. Brennan, "A compact neutron scatter camera for field deployment," *Rev. Sci. Instrum.*, vol. 87, no. 8, p. 083307, 2016.

[11] R. Byrd, "Directional fast-neutron detectors," Los Alamos Nat. Lab., Los Alamos, NM, USA, Tech. Rep. LA-12379-MS, Oct. 1992.

[12] P. A. Marleau, E. Brubaker, G. Mark, A. Nowack, P. Schuster, and J. Steele, "Time encoded radiation imaging," Sandia Nat. Lab., Albuquerque, NM, USA, Tech. Rep. SAND2011-6814, 2011.

[13] W. R. Kaye, N. D. Bennett, C. G. Wahl, Z. He, and W. Wang, "Gamma-ray source location by attenuation measurements," in *Proc. IEEE Nucl. Sci. Symp. Med. Imag. Conf.*, Nov. 2007, pp. 1294–1298.

[14] S. Agostinelli, "GEANT4-a simulation toolkit," *Nucl. Instrum. Methods Phys. Res. A, Accel. Spectrom. Detect. Assoc. Equip.*, vol. 506, no. 3, pp. 250–303, 2003.

[15] Z. He, G. F. Knoll, D. K. Wehe, R. Rojeski, and C. H. Mastraneg, "1-D position sensitive single carrier semiconductor detectors," *Nucl. Instrum. Methods Phys. Res. A, Accel. Spectrom. Detect. Assoc. Equip.*, vol. 380, pp. 228–231, Oct. 1996.

[16] M. Streicher *et al.*, "A portable 2 × 2 digital 3D CZT imaging spectrometer system," in *proc. IEEE Nucl. Sci. Symp. Med. Imag. Conf.*, Nov. 2014, pp. 2–4.

[17] Y. Zhu and Z. He, "Performance of a 2-keV digitizer ASIC for 3-D position-sensitive pixellated semiconductor detectors," in *proc. IEEE Nucl. Sci. Symp. Med. Imag. Conf.*, Nov. 2012, pp. 4109–4112.